ARTICLE

Transparent, Well-Aligned TiO_2 Nanotube Arrays with Controllable Dimensions on Glass Substrates for Photocatalytic Applications

Lee Kheng Tan, Manippady K. Kumar, Wen Wen An,† and Han Gao*

Institute of Materials Research and Engineering, 3 Research Link, Singapore 117602

ABSTRACT Transparent, well-aligned TiO_2 nanotube arrays (NTAs) with controllable dimensions are grown on glass substrates via atomic layer deposition (ALD) of TiO_2 onto free-standing porous anodic alumina (PAA) templates. Photodegradation of aqueous methylene blue (MB) solution and solid stearic acid (SA) film using TiO_2 NTAs of various wall thicknesses are investigated. The Pd functionalized TiO_2 NTAs, with a wall thickness of 15 nm and height of 200 nm, has the highest photodegradation efficiency at 76% after 4 h of UV irradiation. These functionalized NTAs are able to photodegrade MB molecules completely as no obvious demethylated byproducts are observed during the process. It also demonstrates excellent photocatalytic activity for solid contaminants such as SA film. By using the ALD technique, the nanotube wall thickness can be precisely controlled so that it is sufficiently thin to be transparent while sufficiently thick for excellent photocatalytic performances. The transparent TiO_2 NTAs on glass substrates with excellent photocatalytic properties might have potential applications in self-cleaning coating, transparent electronics, and solar cells.

KEYWORDS: photodegradation • transparent TiO_2 film • TiO_2 nanotube arrays (NTAs) • atomic layer deposition (ALD) • porous anodic alumina template (PAA)

INTRODUCTION

TiO_2 nanotube arrays (NTAs) have demonstrated superior performances in a range of applications including dye-sensitized solar cells (1−3), water photoelectrolysis (4−6), hydrogen gas sensing (7−9), photocatalytical conversion of CO_2 to hydrocarbon fuels (10), and photodegradation of organic pollutants (11−15). The superior performances of TiO_2 NTAs are attributed to their unique architectures. For example, compared with nanowires, both external and internal surfaces of the TiO_2 NTAs can be approached by electrolytes. Ultrathin wall thickness, intimate contact with substrates, and well-aligned architecture enable good electrical transport and low charge-carrier recombination (6). In this paper, we are interested in photocatalytic performances of transparent, well-aligned and well-controlled TiO_2 NTAs that are grown on glass substrates. TiO_2 in particulate and film forms has been widely used as photocatalyst (16−18). Transparent TiO_2 films are highly sought after in commercial applications such as photoactive coatings on glass or ceramics substrates (19). Although transparent TiO_2 films on glass substrates are commercially available, the preparation of transparent and vertically well-aligned arrays of TiO_2 nanotubes for photocatalytic applications is still a challenge because of the constraints in fabrication process.

Mohapatra et al. (13) have studied the photocatalytic performances of Pd functionalized TiO_2 NTAs fabricated by anodization of a Ti foil. The NTAs demonstrated good photocatalytic activities that decomposed nonbiodegradable azo dyes completely after a few hours under solar light. Unfortunately, this method is limited by its fabrication process in which TiO_2 NTAs can only be prepared on the Ti foil. Recently, Grimes's group has developed a new method to prepare transparent TiO_2 NTAs on glass substrates via anodization of Ti films deposited on the substrates for dye-sensitized solar cell applications (3, 20). This might be promising for photocatalytic applications where transparency of the product is of importance. It is believed that the thickness and the surface areas of TiO_2 film play critical roles on photocatalytic performances (15). Kemell et al. (14) employed atomic layer deposition (ALD) technique to deposit TiO_2 onto nanoporous alumina membrane and studied their photocatalytic performances. They confirmed that the photodegradation rate of methylene blue (MB) solution was related to the surface areas of the samples. As expected, TiO_2 films show a much slower photodegradation rate than the nanoporous TiO_2 film because the former has a much smaller surface area. However, the nanoporous TiO_2 film is not optically transparent and the process for preparing the nanoporous film results in delaminating, electrolyte contamination and surface modification of the underlying substrate during and after the anodization process (21).

For optimal photocatalytic performances, transparent and vertically well-aligned TiO_2 NTAs with controlled dimensions on transparent substrates are highly desirable. This is mainly due to four positive aspects, namely: (1) TiO_2 NTAs grown on the substrate avoid separation problems which are usually encountered in dispersed TiO_2 nanoparticles/nano-

* To whom correspondence should be addressed. Tel: (65) 6872 7526. Fax: (65) 6772 7744. E-mail: h-gao@imre.a-star.edu.sg.

Received for review October 22, 2009 and accepted February 1, 2010

† Current address: Department of Chemistry, National University of Singapore, Singapore 119077.

DOI: 10.1021/am900726k

Published on Web 02/08/2010

tubes during photodegradation of pollutants (22). (2) Well-aligned and dense open ends of the NTAs allow both their internal and external surfaces to be in contact with the target pollutants (6). (3) Precise control of the wall-thickness of TiO_2 nanotubes reduces recombination of the electron−hole pairs generated by UV irradiation (12). (4) TiO_2 NTAs on transparent substrates such as glass are valuable because of their extensive commercial applications in areas of transparent electronics, and in many photocatalytic applications such as self-cleaning (23, 24), air cleaning (25) and wastewater treatment (26).

Here, we report the photocatalytic activities of transparent, vertically well-aligned and well-controlled TiO_2 NTAs, functionalized with Pd nanoparticles grown on glass substrate. The TiO_2 NTAs are chemically bonded onto the glass substrate. The nanotube wall thickness can be controlled so that it is sufficiently thin to be transparent while sufficiently thick to show excellent photocatalytic activity. This is attributed to the capability of the ALD technique that allows for atomic layer growth of thin films and conformal coating on nanoscaled features (27). The transparent NTAs can photodegrade both aqueous MB solution and solid stearic acid (SA) film under UV irradiation.

EXPERIMENTAL METHODS

ALD of TiO_2 NTAs on Glass Using Free-Standing PAA Template. The procedure has been described elsewhere (21). Briefly, the free-standing PAA template was prepared using a high-purity (99.999%) Al foil (Goodfellow Cambridge) by a two-step anodization. The first anodization was carried out in 0.3 M oxalic acid at room temperature for 6−10 h at 40 V, followed by a second anodization at 2 °C until desired template thickness after removal of the PAA film grown in the first anodized with 3.5 vol % H_3PO_4 and 45 g/L CrO_3 at 60 °C. The as-prepared PAA was subjected to a pore-widening process in 5 wt % H_3PO_4 for 50 min. After that, a protective poly(methyl methacrylate) (PMMA) layer was applied onto the top of the PAA template and dried at 120 °C for 30 min. The template with its protective PMMA layer was separated from the Al substrate using 0.1 M $CuSO_4$ and 10 wt % HCl. The barrier layer at the base of the template was then etched away in 5 wt % H_3PO_4 for another 30−40 min. The PAA template with the PMMA layer was attached onto a glass substrate that was pretreated with O_2 plasma (80 sccm, 80 mTorr, 150 W) prior to the attachment. Finally, the PMMA layer was removed by UV ozone in a dry stripper (Samco UV-1) at 200 °C for 30 min. TiO_2 films were deposited on the whole PAA template attached onto the glass substrate in a viscous flow (1 Torr, 200 sccm N_2 flow) home-built ALD setup at 150 °C. Vapors of $TiCl_4$ (Merck, · 99%) and H_2O precursors were sequentially introduced into the chamber with an exposure time of 0.5 s, and purged by a N_2 flow for 60 s between the two exposures. The TiO_2 overlayer at the top of the template was removed by reactive ion etching (RIE, Oxford Plasmalab 80, 55 sccm CHF_3, 5 sccm O_2) before the NTAs were released from the template in 1 M KOH for 15 min. The NTAs on glass substrate were then annealed in air at 450 °C for 1 h.

Deposition of Pd Nanoparticles. Pd was sputtered at room temperature (Denton Discovery 18 Magnetron Sputtering system) onto the as-annealed TiO_2 NTAs for 4 s from a high-purity Pd target (99.999%), at a sputtering power of 100 W, a working pressure of 5 mTorr, as well as an air flow of 10 sccm. Pd nanoparticles were obtained by an activation procedure performed in a tubular quartz chamber. The activation procedure involved a heat treatment of the sample to 300 °C in hydrogen (1000 ppm H_2 in N_2 balance) at atmospheric pressure for 2 min and thereafter 3 cycles of air and hydrogen exposures. The gas flow rate into the chamber was 500 sccm during the entire process. The activation process was closely monitored by the electrical conduction measurements of the Pd overlayer. The conductivity decreased sharply because of the segregation of the Pd overlayer leading to the formation of Pd nanoparticles.

Photodegradation of MB Solution and SA Film. The 2.5 cm × 2 cm samples were immersed in unstirred MB ($C_{16}H_{18}ClN_3S \cdot xH_2O$, Sigma-aldrich) solution, with an initial concentration of $C_o = 1.0 \times 10^{-5}$ M, for an hour each time under UV irradiation (Hamamatsu UV spot lightsource LC5, maximum 365 nm, ∼1.25 mW/cm^2). The MB concentration after UV irradiation was measured using a UV−vis−NIR scanning spectrophotometer at wavelength of 665 nm. Five microliters of 8.8×10^{-3} M SA in methanol solution (Fluka · 97%) was spin-coated (2 min, 1000 rpm) onto the TiO_2 samples. The TiO_2 samples were exposed to UV irradiation for 3 h to remove other contaminants prior to SA spin-coating. The photodegradation of solid SA films with FTIR peaks at 2849 and 2916 cm^{-1} were measured in a transmission mode after every 10 or 30 min of UV irradiation.

Characterization. Field emission scanning electron microscopy (FESEM, JEOL 6700F) was used to characterize morphology of the PAA template and TiO_2 NTAs on glass substrate. High-resolution transmission electron microscopy (HRTEM, Philips CM300) was used to study the structure of the TiO_2 NTAs. The sample for cross-sectional HRTEM was prepared by bonding the top surfaces of 2 pieces of 3 mm × 1 mm samples with epoxy glue. The sample was cured and subsequently polished using graphite lapping film until about 10−50 μm thick. The sample was dimpled and finally ion milled until transparent. UV−vis spectra for photodegradation of MB solution was analyzed using UV−vis−NIR scanning spectrophotometer (Shimadzu UV 3101) and FTIR spectra for photodegradation of SA film was analyzed using Fourier-transform infrared spectrometer (FT-IR, Perkin-Elmer).

RESULTS AND DISCUSSIONS

The TiO_2 thin film was deposited by ALD onto a free-standing PAA template which was attached onto a glass substrate. TiO_2 NTAs were released from the template by chemical etching. Figure 1a shows a SEM image of a free-standing PAA template firmly attached onto the glass substrate. The pores of the template are hexagonally packed with a diameter of 65 nm, a height of 200 nm and an interpore spacing of 110 nm. The shape, size, height and interpore spacing of these pores can be well-controlled by varying the anodization conditions (28−30). Figure 1b displays transparent, dense, and well-aligned TiO_2 NTAs on the glass substrate, which have been released from the PAA template. The NTAs shown here are of 200 nm in height and 15 nm in wall thickness. The growth rate of TiO_2 film is ∼1 Å/cycle. The dimensions of the TiO_2 NTAs can be controlled by correspondingly varying dimensions of the PAA template while their wall-thickness is determined by the number of ALD cycles. The nanotube wall-thickness plays a crucial role on charge transfer and separation of electron−hole pairs during photocatalysis (14). As such, the ALD technique allows us to control the wall thickness so it is thick enough to exhibit high photocatalytic performance and thin enough to have a good transparency in the visible spectrum. Figure 1c shows an oblique view of the TiO_2 NTAs with intimate

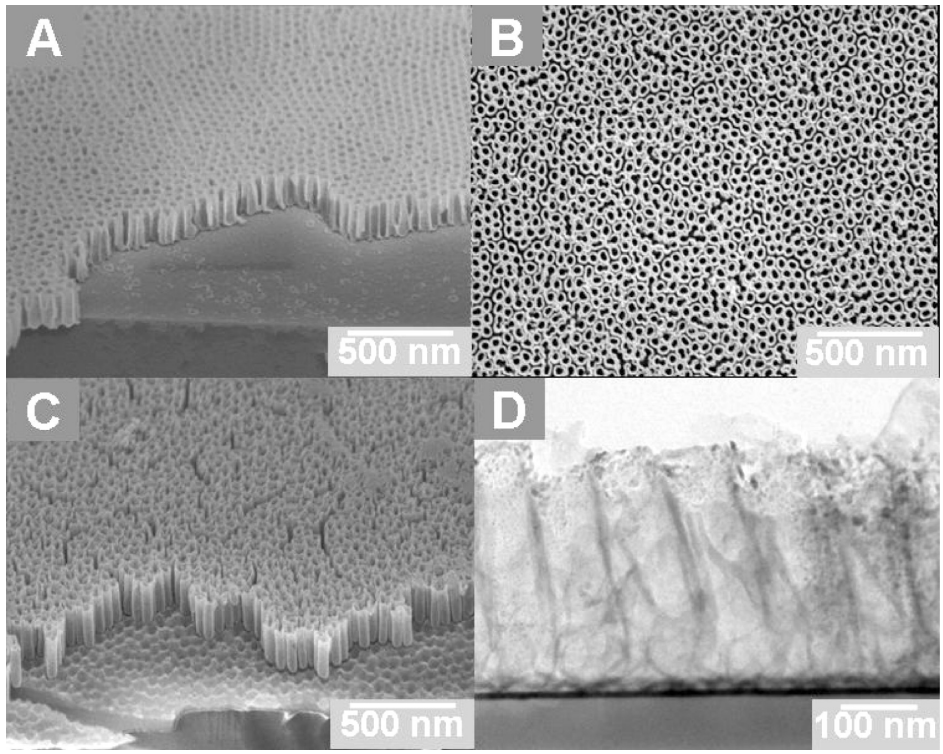

FIGURE 1. Nanoporous free-standing PAA template and TiO_2 NTAs on the glass substrates. (A) SEM image of a free-standing PAA template adhering to the glass substrate. Uniform, hexagonally packed pores with an average diameter of 65 nm and interpore spacing of 110 nm. (B) Top-view SEM image of dense and vertically well-aligned TiO_2 NTAs on glass substrate after being released from the PAA template. The NTAs are 200 nm in height and 15 nm in wall thickness. (C) Oblique SEM image revealing TiO_2 NTAs intimately attached onto the glass substrate even after cleavage of the substrate. The NTAs are assumed to be chemically bonded onto the glass substrate. (D) Cross-sectional HRTEM of TiO_2 NTAs on the glass substrate functionalized with Pd nanoparticles that act as a catalyst for photocatalytic reactions.

contact with the glass substrate, even after cleavage in preparation for SEM observance. The intimate contact between the NTAs and the glass substrate is due to the chemical bonding at the interface of the first layer of TiO_2 film and the glass substrate. Figure 1d demonstrates the cross-sectional HRTEM image of Pd nanoparticles functionalized TiO_2 NTAs on the glass substrate. The excellent adhesion between the attached NTAs and the glass substrate is further illustrated in this image. The adhesion can be improved by O_2 plasma treatment on the glass substrate prior to the attachment of PAA template. Pd nanoparticles, with sizes ranging from 10 to 20 nm, are found mostly dispersed on the top of the NTAs. They act as catalysts to promote the photocatalytic reactions (31), by improving the rate of reduction of oxygen and preventing electron−hole recombination.

The photo image of the glass substrate covered with Pd-functionalized TiO_2 NTAs is shown in Figure 2a. It is clearly evident that the whole sample is uniform and optically transparent, with the logo of A*STAR being seen underneath the glass substrate. The transmittance spectra of a blank glass substrate and a glass substrate covered with Pd functionalized TiO_2 NTAs are shown in Figure 2b. In the visible spectrum, there is not much major difference in transmittance between the two samples. The transmittance of the 15 nm thick walled, Pd-functionalized NTAs is up to 90%. The anatase TiO_2 NTAs are obtained by 450 °C annealing for 1 h (21).

The photodegradation behaviors of 1.0×10^{-5} M MB solution using TiO_2 films and NTAs functionalized with and without Pd nanoparticles are compared in Figure 3. A blank glass substrate without any coatings was used as a control sample. Figure 3a compares the kinetic curves of MB photodegradation between different TiO_2 structures (films and NTAs), of different thickness (10, 15, 20 nm) and those with and without functionalization of Pd nanoparticles. Except for 10 nm NTAs without Pd nanoparticles and 10 nm TiO_2 NTAs with Pd nanoparticles, it is apparent that the photodegradation of MB solution obeys first-order reaction kinetic. The photodegradation efficiencies for all samples in MB solution under 4 h UV irradiation are shown in Figure 3b and summarized in Table 1. Among the TiO_2 films, the 15 nm film demonstrates the best photodegradation efficiency, with 58% of MB photodegraded, whereas the 10 nm thick film has only 37% of MB photodegraded. A further increase in film thickness at 20 nm thick does not improve the photocatalytic performance. It can also be seen that, among TiO_2 NTAs without Pd nanoparticles, NTAs with a 15 nm thick wall shows the highest photodegradation efficiency at 62%, which is higher than that of the film sample with a similar thickness. Furthermore, Pd-functionalized NTAs with the same wall thickness have 76% of MB photodegraded and have the highest photodegradation efficiency among all the samples. This might be ascribed to the high surface areas including internal surfaces, catalysis of Pd nanoparticles, and an appropriate wall thickness that allows for more effective

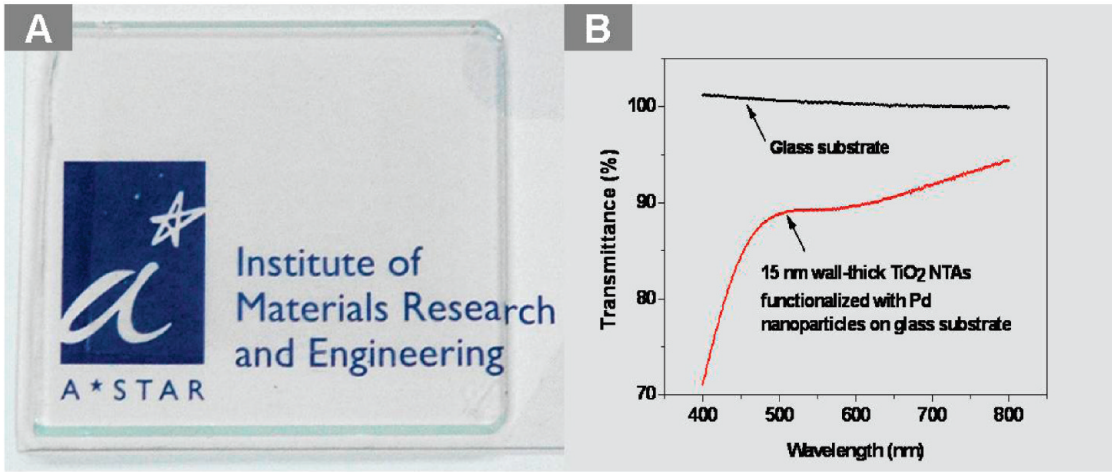

FIGURE 2. Transparent TiO_2 NTAs on the glass substrate. (A) Background logo of A*STAR is clearly seen underneath the transparent NTAs on the glass substrate. (B) Transmittance spectra of a blank glass substrate and Pd-functionalized, 15 nm thick walled NTAs on the glass substrate. No significant difference in transmittance between the glass and the glass with NTAs in the visible spectrum. The transmittance of the Pd-functionalized NTAs is up to 90%.

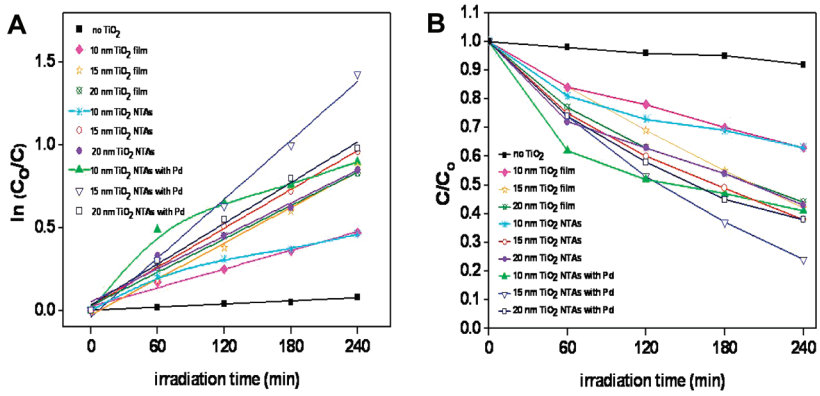

FIGURE 3. Kinetic plots of photocatalytic degradation of 1.0×10^{-5} M MB solution using TiO_2 films and NTAs under UV irradiation. The highest photodegradation efficiency at 76% of MB photodegraded after 4 h UV irradiation is observed for Pd-functionalized TiO_2 NTAs with a wall thickness of 15 nm.

Table 1. Percentage of 1.0×10^{-5} M MB Solution Photodegraded after 4 h UV Irradiation

TiO_2 nanostructures	percentage of photodegradation (%)
10 nm TiO_2 film	37
15 nm TiO_2 film	58
20 nm TiO_2 film	56
10 nm TiO_2 NTAs	37
15 nm TiO_2 NTAs	62
20 nm TiO_2 NTAs	57
10 nm TiO_2 NTAs with Pd	59
15 nm TiO_2 NTAs with Pd	76
20 nm TiO_2 NTAs with Pd	62
no TiO2	8

separation of the electron−hole (14, 31, 32). Moreover, the ALD technique precisely controls the film thickness, which optimized the wall thickness of TiO_2 nanotubes on the glass substrate, resulting in high photocatalytic performances.

Figure 4 shows a series of UV−vis absorption spectra of 1×10^{-5} M MB solution photodegraded by Pd functionalized TiO_2 NTAs with a wall thickness of 15 nm, recorded with increasing UV irradiation time. It was reported that there were two competitive reactions in the process of MB photodegradation, i.e., photodegradation and demethylation (17). The demethylation is characterized by the blue-shift of the absorption peak at 660 nm in the UV−vis absorption spectrum. In Figure 4, the intensity of the maximum absorption peak at 660 nm decreased with increasing UV irradiation time because of the degradation of MB solution, but less

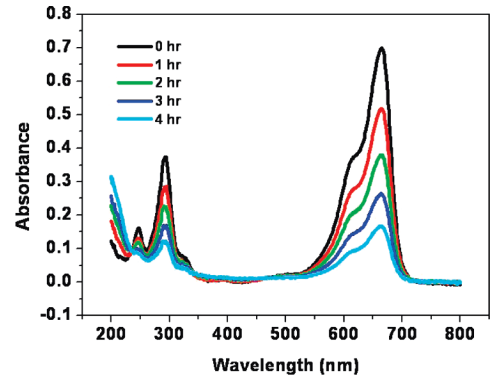

FIGURE 4. UV−vis absorption spectra of MB solution photodegraded by Pd-functionalized, 15 nm thick walled TiO_2 NTAs under UV irradiation. Maximum absorption peak at 660 nm decreased as a function of UV irradiation time with no apparent blue-shift observed.

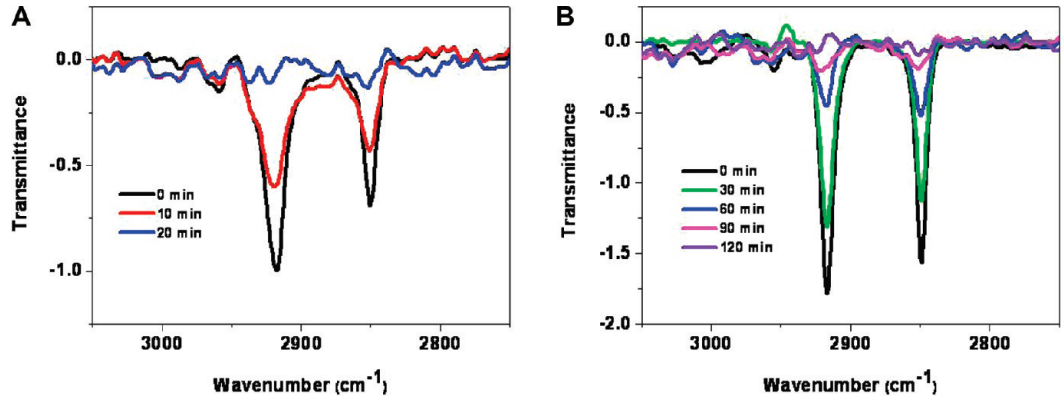

FIGURE 5. FTIR transmittance spectra of photodegradation of SA film coated onto 15 nm thick walled, Pd-functionalized TiO_2 NTAs and a 15 nm thick TiO_2 film on glass substrates. The two SA peaks at 2916 and 2849 cm^{-1} disappeared after 20 min UV irradiation for NTAs substrate, whereas they disappeared after only 120 min UV irradiation for film substrate.

blue-shift was observed, indicating complete photodegradation of the MB solution.

Besides photodegradation of MB aqueous solution, we have also investigated the photocatalytic activity of solid contaminants such as SA films (33). Specifically, TiO_2 film and Pd-functionalized NTAs, with the same thickness of 15 nm on glass substrate, were investigated. The SA in methanol solution was spin-coated onto the substrates. Infrared adsorption spectroscopy was used to monitor the decomposition of SA films as SA shows strong absorption in the region of 2700 − 3000 cm^{-1}. Figure 5a,b displays the FTIR spectra, with increasing UV irradiation time, for the photodegradation of SA on the TiO_2 NTAs and film, respectively. The two transmittance peaks at 2916 and 2849 cm^{-1} are attributed to asymmetric and symmetric C−H stretching in $-CH_2$ groups, respectively (34). In Figure 5a, it is obvious that both peaks disappeared after 20 min UV irradiation. However, the disappearance of the same peaks, as seen in Figure 5b, occurs after only 120 min UV irradiation. This result indicates that the TiO_2 NTAs demonstrate far better photocatalytic activity than the TiO_2 film under similar conditions. This is ascribed to the larger surface areas of the NTAs as compared with film architecture. As such, besides photodegradation of aqueous MB solution, the TiO_2 NTAs on glass substrate can photodegrade solid SA film. Compared with its film counterpart, nanotube architecture demonstrates far better photocatalytic activities.

CONCLUSIONS

In summary, we have prepared transparent and well-aligned TiO_2 NTAs on glass with controllable dimensions. The TiO_2 NTAs are chemically bonded on the glass substrate. The photocatalytic activities of the NTAs were studied using both MB aqueous solution and SA solid films under UV irradiation. Because of the precise film thickness control by the ALD technique, we are able to grow the TiO_2 NTAs with an optimal wall thickness that is sufficiently thin for the surface to be transparent while sufficiently thick to show excellent photocatalytic activities. The Pd functionalized TiO_2 NTAs with a wall thickness of 15 nm was found to have the highest photocatalytic activity in MB solution. This transparent TiO_2 NTAs grown on the glass substrate can also photodegrade solid SA film. As compared with TiO_2 thin film, TiO_2 NTAs demostrate higher photocatalytic activity because of their higher surface areas. It is worth noting that besides growing on the glass substrate, our method can also be applied to grow NTAs on other types of substrates, such as polymers, as a photocatalytic protective layer on transparent and flexible electronics.

Acknowledgment. We thank the Institute of Materials Research and Engineering under the Agency for Science, Technology and Research (A*STAR), Singapore, for the financial support. We thank Tan Hui Ru for her assistance with HRTEM.

REFERENCES AND NOTES

(1) Kang, T. S.; Smith, A. P.; Taylor, B. E.; Durstock, M. F. *Nano Lett.* **2009**, *9*, 601.
(2) Paulose, M.; Shankar, K.; Varghese, O. K.; Mor, G. K.; Grimes, C. A. *J. Phys. D: Appl. Phys.* **2006**, *39*, 2498.
(3) Varghese, O. K.; Paulose, M.; Grimes, C. A. *Nat. Nanotechnol.* **2009**, *4*, 592.
(4) Mohapatra, S. K.; Misra, M.; Mahajan, V. K.; Raja, K. S. *J. Phys. Chem. C* **2007**, *111*, 8677.
(5) Nam, W.; Han, G. Y. *J. Chem. Eng. Jpn.* **2007**, *40*, 266.
(6) Shankar, K.; Basham, J. I.; Allam, N. K.; Varghese, O. K.; Mor, G. K.; Feng, X. J.; Paulose, M.; Seabold, J. A.; Choi, K. S.; Grimes, C. A. *J. Phys. Chem. C* **2009**, *113*, 6327.
(7) Mor, G. K.; Varghese, O. K.; Paulose, M.; Grimes, C. A. *Sens. Lett.* **2003**, *1*, 42.
(8) Mor, G. K.; Carvalho, M. A.; Varghese, O. K.; Pishko, M. V.; Grimes, C. A. *J. Mater. Res.* **2004**, *19*, 628.
(9) Varghese, O. K.; Mor, G. K.; Grimes, C. A.; Paulose, M.; Mukherjee, N. *J. Nanosci. Nanotechnol.* **2004**, *4*, 733.
(10) Varghese, O. K.; Paulose, M.; LaTempa, T. J.; Grimes, C. A. *Nano Lett.* **2009**, *9*, 731.
(11) Lai, Y. K.; Sun, L.; Chen, Y. C.; Zhuang, H. F.; Lin, C. J.; Chin, J. W. *J. Electrochem. Soc.* **2006**, *153*, D123.
(12) Liang, H. C.; Li, X. Z. *J. Hazard. Mater.* **2009**, *162*, 1415.
(13) Mohapatra, S. K.; Kondamudi, N.; Banerjee, S.; Misra, M. *Langmuir* **2008**, *24*, 11276.
(14) Kemell, M.; Pore, V.; Tupala, J.; Ritala, M.; Leskela, M. *Chem. Mater.* **2007**, *19*, 1816.
(15) Heikkia, M.; Puukilainen, E.; Ritala, M.; Leskela, M. *J. Photochem. Photobiol., A* **2009**, *204*, 200.
(16) Lakshmi, S.; Renganathan, R.; Fujita, S. *J. Photochem. Photobiol., A* **1995**, *88*, 163.
(17) Yogi, C.; Kojima, K.; Wada, N.; Tokumoto, H.; Takai, T.; Mizoguchi, T.; Tamiaki, H. *Thin Solid Films* **2008**, *516*, 5881.
(18) Straka, L.; Kawakami, H.; Romu, J.; Ilola, R.; Mahlberg, R.; Heikkila, M.; Hanninen, H. *Thin Solid Films* **2009**, *517*, 3797.
(19) Mills, Andrew; Soo Keun, Lee *J. Photochem. Photobiol., A* **2002**, *152*, 233.

(20) Mor, G. K.; Varghese, O. K.; Paulose, M.; Grimes, C. A. *Adv. Funct. Mater.* **2005**, *15*, 1291.
(21) Tan, L. K.; Chong, M. A. S.; Gao, H. *J. Phys. Chem. C* **2008**, *112*, 69.
(22) Hoffmann, M. R.; Martin, S. T.; Choi, W.; Bahnemann, D. W. *Chem. Rev.* **2002**, *95*, 69.
(23) Parkin, I. P.; Palgrave, R. G. *J. Mater. Chem.* **2005**, *15*, 1689.
(24) Euvananont, C.; Junin, C.; Inpor, K.; Limthongkul, P.; Thanachayanont, C. *Ceram. Int.* **2008**, *34*, 1067.
(25) Fujishima, A.; Zhang, X. T. *C. R. Chim.* **2006**, *9*, 750.
(26) Ghezzar, M. R.; Abdelmalek, F.; Belhadj, M.; Benderdouche, N.; Addou, A. *J. Hazard. Mater.* **2009**, *164*, 1266.
(27) Knez, M.; Niesch, K.; Niinisto, L. *Adv. Mater.* **2007**, *19*, 3425.
(28) Li, A. P.; Muller, F.; Birner, A.; Nielsch, K.; Gosele, U. *J. Appl. Phys.* **1998**, *84*, 6023.
(29) Lee, W.; Ji, R.; Gosele, U.; Nielsch, K. *Nat. Mater.* **2006**, *5*, 741.
(30) Masuda, H.; Fukuda, K. *Science* **1995**, *268*, 1466.
(31) Kovalenko, N.; Petkevich, T.; Egiazarov, Yu *J. Appl. Spectrosc.* **1999**, *66*, 88.
(32) Zhuang, H. F.; Lin, C. J.; Lai, Y. K.; Sun, L.; Li, J. *Environ. Sci. Technol.* **2007**, *41*, 4735.
(33) Mills, A.; McFarlane, M. *Catal. Today* **2007**, *129*, 22.
(34) Sawunyama, P.; Jiang, L.; Fujishima, A.; Hashimoto, K. *J. Phys. Chem. B* **1997**, *101*, 11000.

AM900726K